The Astrophysical Journal, 740:62 (7pp), 2011 October 20 doi:10.1088/0004-637X/740/2/62

RADIATIVE HEATING OF THE SOLAR CORONA

Thomas G. Moran
Physics Department, Catholic University of America, 200 Hannan Hall,
Washington, DC 20064, USA; moran@grace.nascom.nasa.gov
and
NASA/GSFC, Code 671, Greenbelt, MD 20771, USA
Received 2011 February 11; accepted 2011 July 5; published 2011 September 30

ABSTRACT

We investigate the effect of solar visible and infrared radiation on electrons in the Sun's atmosphere using a Monte Carlo simulation of the wave–particle interaction and conclude that sunlight provides at least 40% and possibly all of the power required to heat the corona, with the exception of dense magnetic flux loops. The simulation uses a radiation waveform comprising 100 frequency components spanning the solar blackbody spectrum. Coronal electrons are heated in a stochastic manner by low coherence solar electromagnetic radiation. The wave "coherence time" and "coherence volume" for each component is determined from optical theory. The low coherence of solar radiation allows moving electrons to gain energy from the chaotic wave field which imparts multiple random velocity "kicks" to these particles causing their velocity distribution to broaden or heat. Monte Carlo simulations of broadband solar radiative heating on ensembles of 1000 electrons show heating at per particle levels of 4.0×10^{-21} to 4.0×10^{-20} W, as compared with non-loop radiative loss rates of $\approx 1 \times 10^{-20}$ W per electron. Since radiative losses comprise nearly all of the power losses in the corona, sunlight alone can explain the elevated temperatures in this region. The volume electron heating rate is proportional to density, and protons are assumed to be heated either by plasma waves or through collisions with electrons.

Key words: solar wind – Sun: atmosphere – Sun: chromosphere – Sun: corona – Sun: fundamental parameters – Sun: heliosphere

1. INTRODUCTION

The region surrounding the Sun made visible during total solar eclipses is known as the corona and is one of the most intriguing features of our star. The magnetic energy release events known as solar flares and coronal mass ejections which can affect Earth and its near-space environment occur in the corona. This region is also the origin of the supersonic solar wind, which bathes Earth in a constant plasma flow and may receive its energy from the corona. Therefore, determining the physical conditions and drivers in the corona is crucial for understanding the Sun's affect on the Earth. Among the most important coronal characteristics is its temperature. In 1942, it was discovered that several spectral lines emitted by the corona were radiated by highly ionized iron and calcium, which can only exist in a plasma with a temperature of at least 1×10^6 K (Edlen 1943). A discussion of the history surrounding this discovery can be found in Phillips (2000). The corona is much hotter than the photosphere, which has a temperature of 5800 K. Since the temperature at the surface of the Sun, the source of the corona's energy, is much lower than the coronal value, it cannot be heated by thermal conduction. There must be a nonconductive heating mechanism.

Some basic characteristics of the coronal heating mechanisms can be inferred from observations showing that the temperature varies slowly in time and space in regions where the density varies smoothly, indicating that the heating must extend throughout the region with little spatial or temporal variation except in regions with strong density gradients. Vigorous efforts to determine how the corona is heated have focused on nonthermal mechanisms which satisfy these requirements (Phillips 2000; Aschwanden 2001b). In spite of the considerable attempts to deduce the cause or causes of the high coronal temperatures, it has remained unknown. This has motivated our investigation of heating of the coronal plasma by solar electromagnetic radiation, a nonconductive mechanism which is nearly constant in time and varies slowly in space. The radiation intensity in the corona is high, with peak values of 6.6×10^7 W m^{-2} near the surface, and are a factor of $\approx 10^5$ larger than estimated required coronal power levels, as demonstrated in Section 5. Therefore, only a small fraction of solar electromagnetic radiation must be converted to heat in order to explain coronal temperatures.

Radiative heating of the inner solar atmosphere by continuum and spectral line emission has been investigated and it was found that under certain simplifying assumptions a temperature rise is predicted above the photosphere consistent with the existence of a hot chromosphere (Cayrel 1964, 1966; Mihalas 1978). Modeling of the solar chromospheric radiative energy balance showed that heating by absorption of hydrogen Lyα and Balmer continuum radiation provides part of the power required to balance losses (Vernazza et al. 1981). Chromospheric heating by the absorption of electromagnetic waves that originate from the photospheric blackbody radiation has also been investigated (Tsiklauri & Pechhacker 2011). The absorption is provided by the electron–neutral collisions in which electrons oscillate in the wave field and electron–neutral collisions damp the wave. Given the uncertain nature of the collision cross section due to the plasma microturbulence, it is shown that for plausible physical parameters, the heating flux produced by the absorption of radiation in the chromosphere is between 20% and 45% of the heat required.

We investigate a stochastic radiative coronal heating mechanism by which "partially coherent" solar electric wave fields cause multiple random velocity "kicks" to moving electrons, increasing mean particle speeds and temperatures to their coronal values. The possibility of this heating depends upon a property of light known as "coherence," which is the spatial or temporal extent over which waves are approximately in phase. We simulate this process using a Monte Carlo method incorporating coherence characteristics predicted by optical theory. From this

analysis, we find that radiative heating supplies at least 40% of the power required to balance radiative losses and might provide all of the power necessary to satisfy coronal requirements.

We present the basic theory of optical coherence in Section 2 and the stochastic radiative heating in Section 3. We then compare the predictions of the theory with coronal heating requirements in Section 4. Our conclusions are presented in Section 5 and a discussion of the results is presented in Section 6.

2. SOLAR RADIATION COHERENCE

There are two types of optical coherence: temporal and spatial (Wolf 2007; Mandel & Wolf 1995). Furthermore, there are two types of spatial coherence: transverse and longitudinal. Coherence is described by either a "coherence length" or "coherence time," over which radiation maintains a predictable phase relationship. Sunlight is an example of a radiation field with limited coherence. Solar visible and infrared radiation arises from many spatially separated random uncorrelated electron–atom recombination events which produce negative hydrogen ions (Chandrasekhar 1989). These recombination events produce wavetrains which overlap in the corona, resulting in a field with a low level of spatial and temporal coherence. To determine the effect of solar radiation on the corona, we must know the coherence time of this field.

The standard expression for the coherence time τ_c of a wave field with a bandwidth of $\Delta\nu$ was derived from Fourier analysis under the implicit assumption that phase is independent of wavelength: $\tau_c = (\Delta\nu)^{-1}$ (Mandel & Wolf 1995). Since $\nu \approx \Delta\nu$ for the solar spectrum, this yields $\tau_c \approx \tau_w$, where τ_w is the wave period. However, it would not be appropriate to use a single value for τ_c for all frequencies for several reasons. To define a wave, there must be at least one minimum and one maximum. If $\tau_c < \tau_w$ the wave is not coherent for a full period and the wavelength and frequency cannot be defined. Furthermore, if $\tau_c = 1.5\,\tau_w$, the wave field is not balanced over a coherence time, which would not be physical and would lead to unbalanced driving of free charge particles. Therefore, if the Fourier analysis treatment for coherence time is adopted, one should assume that $\tau_c \approx \tau_w$ for each frequency.

The conclusion that $\tau_c \approx \tau_w$ also results from the analysis of Agarwal et al. (2004), who computed the degree of coherence as a function of angle for a sphere of incoherent monochromatic emitters in the near-field case. They found that the coherence function and coherence length they derived agreed with that yielded by the far-field treatment for distances greater than 10 wavelengths from the surface, with the coherence length l_t given by $l_t \approx \lambda$. From this they concluded that the far-field assumption was likely to also be valid in the case of solar radiation close to the Sun. We will assume that this relation applies at each wavelength. Since light propagation directions from disk center and the limb are approximately perpendicular in the low corona, we will assume that the longitudinal coherence length l_l is given by $l_l \approx l_t$. We define the "geometric coherence time" as the effective coherence time in case of infinite source coherence time. The geometric coherence time is then given by $\tau_c \approx l_l/c$, where c represents the speed of light, so that $\tau_c \approx \tau_w$. Given that there are no measurements of coherence time in the corona, we will assume this value for τ_c. Therefore sunlight is assumed to be coherent over a spherical volume of diameter $\approx \lambda$. We may consider the corona to comprise multiple adjacent "coherence cells," with centers separated by λ. The geometric coherence time, τ_c, is approximately equal to the wave period, $\tau_c \approx \tau_w = l_l/c$.

In general, the coherence time is determined by both the geometric and source coherence times. But if one coherence time is much shorter than the other, then the lower value will equal the effective coherence time. The source coherence time is determined by the electron–hydrogen atom recombination process which creates sunlight (Chandrasekhar 1989). We may determine a lower limit to the source coherence time from solar observations at 1 AU using the Fourier Transform Spectrograph (FTS) at the McMath–Pierce Telescope at the National Solar Observatory at Kitt Peak. The FTS varies the path difference between two solar beams from 0 m to 0.5 m and recombines the beams to obtain an interferogram that is inverted to yield the solar spectrum between 2000 Å and 30 μm (Ridgway & Brault 1984). From these measurements, a lower limit on the source coherence time τ_{sc} may be calculated: $0.5\,\mathrm{m}/c$, where c is the speed of light. This yields a lower limit for τ_{sc} of 1.6×10^{-9} s. Since $\tau_c \ll \tau_{sc}$, the effective coherence time in the corona equals τ_w.

The effect of solar radiation on coronal electrons will depend on whether the field is fully "chaotic" at the electron's position. In this case, the electric field at any time is independent of the electric field in the past. This is not the case for any fixed coronal position. The light at a given coronal location comprises multiple overlapping wavetrains resulting from uncorrelated separated recombination events on the disk. Since $\tau_c \ll \tau_{sc}$, the field will be pseudochaotic over times much less than τ_{sc}. But over times large compared with τ_{sc}, it will average to zero since the time integral of a single wavetrain field equals zero, and therefore the field will not be fully chaotic. However, we must also consider the effect of the electron's motion. A moving electron transits a coherence cell in a transit time, τ_{tr} given by $\tau_{tr} = \lambda/v$, where v is the electron speed. If $\tau_{tr} \ll \tau_{sc}$, the field at the electron will be chaotic. For a coronal electron thermal speed of $6 \times 10^6\,\mathrm{m\,s^{-1}}$ and a mean solar wavelength of 5000 Å $\tau_{tr} = 8.3 \times 10^{-14}$ s as compared with a minimum value of τ_{sc} of 5×10^{-9} s. Therefore, $\tau_{tr} \ll \tau_{sc}$, implying that the radiation field at the electron is chaotic in the electron's frame and radiation of a given wavelength comprises a series of wavepackets of random phase, each defined by a Gaussian envelope with a width of $\approx\tau_w$, and separated in time by an interval of $\approx\tau_w$.

3. THEORY OF RADIATION-DRIVEN ELECTRON VELOCITY SPACE DIFFUSION

As demonstrated in Section 4, the partially coherent solar radiation field imparts a series of random velocity kicks to coronal electrons. In order to understand the effect of this radiation, we will demonstrate how random kicks cause diffusion and broadening of the electron velocity distribution. This analysis will yield the theoretical electron heating rate resulting from radiation-driven velocity diffusion.

The evolution and heating of the electron distribution is determined by the velocity space diffusion coefficient, D_v. The three-dimensional diffusion coefficient D_v is given by

$$D_v = \frac{1}{6}\frac{\delta v^2}{\tau_c} \tag{1}$$

where δv is the velocity kick since there is one kick per coherence time τ_c. We assume that the electron velocity distribution is represented by $F(v)$, where v is the particle speed: $F(v)$ is a function only of the electron speed. The normalization condition

is given by

$$\int_0^\infty F(v)\,4\pi\,v^2\,dv = 1 \tag{2}$$

since the angular component of the integral equals 4π. Ignoring non-wave influences on velocity, we can express the diffusive component of the time derivative of $F(v)$ under the assumption of isotropic diffusion as

$$\frac{dF(v)}{dt} = D_v\left(\frac{d^2F(v)}{dv^2} + \frac{2}{v}\frac{dF(v)}{dv}\right). \tag{3}$$

The mean kinetic of a coronal electron, $\langle U_e\rangle$, is given by the average of the particle energy $(1/2)\,m_e\,v^2$:

$$\langle U_e\rangle = \int_0^\infty F(v)\,\frac{m_e v^2}{2}\,4\pi\,v^2\,dv. \tag{4}$$

As diffusion broadens the distribution, the stochastic radiative heating rate per particle from solar radiation, H_e, is given by

$$H_e = \frac{d\langle U_e\rangle}{dt} \tag{5}$$

and therefore, from Equation (4),

$$H_e = \frac{m_e}{2}\int_0^\infty \frac{dF(v)}{dt}\,4\pi\,v^4\,dv. \tag{6}$$

From Equation (3), we may then express H_e as

$$H_e = \frac{m_e}{2}\int_0^\infty D_v\left(\frac{d^2F(v)}{dv^2} + \frac{2}{v}\frac{dF(v)}{dv}\right)4\pi\,v^4\,dv. \tag{7}$$

We may further express H_e as

$$H_e = \frac{D_v m_e}{2}\,G, \tag{8}$$

where G is the definite integral given by

$$G = \int_0^\infty \left(\frac{d^2F(v)}{dv^2} + \frac{2}{v}\frac{dF(v)}{dv}\right)4\pi\,v^4\,dv. \tag{9}$$

The integral G may be evaluated by parts using the normalization condition given in Equation (2) if $(v^4\,F(v),\ v^3\,dF(v)/dv) \to 0$ as $v \to \infty$, yielding $G = 9$. From Equation (8), we may then express H_e as

$$H_e = 4.5\,m_e\,D_v. \tag{10}$$

4. SIMULATION OF ELECTRON VELOCITY DIFFUSION AND HEATING IN THE SOLAR RADIATION FIELD

4.1. Electron Motion Simulation in the Low Coherence Solar Radiation Field

Consider the effect of a monochromatic beam of light of amplitude, E, circular frequency, ω, and phase δ,

$$E = E_o\,\sin(\omega t + \delta), \tag{11}$$

where $\omega = \nu/2\pi$, ν is the frequency, and t is the time. In the one-dimensional case, the field exerts a force on a free charged particle of mass m and charge q, with the resulting velocity v determined by the momentum equation

$$m\frac{dv}{dt} = q\,E_o\,\sin(\omega t + \delta). \tag{12}$$

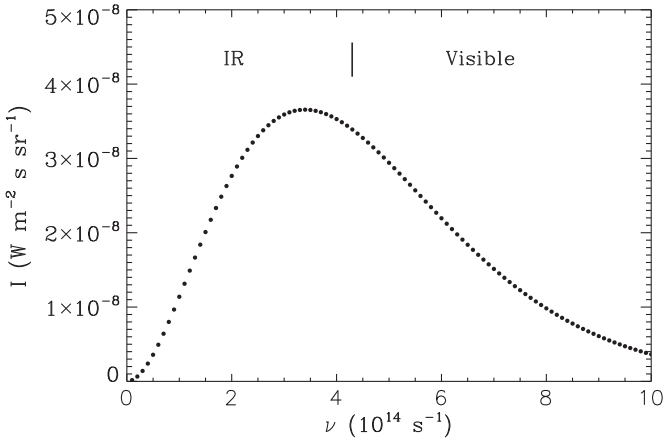

Figure 1. Solar blackbody intensity I_{ν_i} component amplitudes plotted vs. frequency ν. The infrared (IR) and visible ranges of the spectrum are indicated.

The field will cause a sinusoidal motion, with the magnitude of v given by

$$v = \frac{q\,E_o}{m\omega}. \tag{13}$$

Thus, electron speeds will be greater than proton speeds by a factor of the proton–electron mass ratio, 1836, and so we ignore the proton motion and set $q = e$ and $m = m_e$, where m_e represents the electron mass.

The wave amplitude E_o is related to the Poynting vector, S_o, by

$$S_o = \frac{c\,\epsilon_o}{2}\,E_o^2, \tag{14}$$

where ϵ_o is the electric permittivity, equal to $8.85\times10^{-12}\,\mathrm{F\,m^{-1}}$. The field strength, E_o, is then given by

$$E_o = \left(\frac{2\,S_o}{\epsilon_o\,c}\right)^{-1/2}. \tag{15}$$

The Poynting vector in the corona is determined by the solar disk irradiance. This is the intensity of light radiated by the photosphere into the corona, which is given by the relation

$$S_o = \sigma_{\mathrm{SB}}\,T_s^4\,r_n^{-2}, \tag{16}$$

where σ_{SB} is the Stefan–Boltzmann constant, equal to $5.67\times10^{-8}\,\mathrm{W\,m^{-2}\,K^{-4}}$ and T_s is the solar surface temperature, equal to 5800 K and r_n is the normalized heliocentric distance. This formula yields a value of S_o of $1366\,\mathrm{W\,m^{-2}}$ at 1 AU, as it should. In addition, the solar spectrum measured at 1 AU follows at blackbody spectrum for $T_s = 5800$ K. At wavelengths less than 3000 Å or frequencies greater than $1\times10^{15}\,\mathrm{s^{-1}}$, the corona is not optically thin owing to resonance absorption and therefore the spectrum in that range is not given by the blackbody distribution. However, the emission in the extreme ultraviolet comprises less than 1% of the solar irradiance and we may ignore that radiation in our investigation. The value of S_o at the coronal base is $6.6\times10^7\,\mathrm{W\,m^{-2}}$, which corresponds to a field strength amplitude E_o of $2.2\times10^5\,\mathrm{V\,m^{-1}}$. The rms field strength E_{rms} is given by $E_{\mathrm{rms}} = 0.7\,E_o$.

To simulate the effect of solar radiation on electrons, we decompose the blackbody solar spectrum into 100 spectral components, at frequencies ν_i given by $\nu_i = i\,1.0\times10^{13}\,\mathrm{s^{-1}}$ where i covers the range (1, 100). A plot of the spectrum between $\nu = 0$ and $\nu = 1.0\times10^{15}\,\mathrm{s^{-1}}$ is shown in Figure 1. The

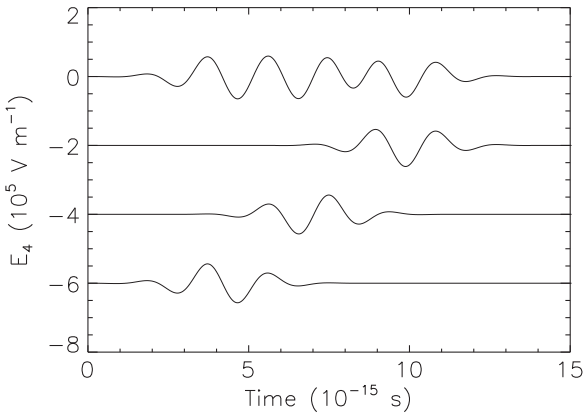

Figure 2. Plots of three wavepackets of frequency $5 \times 10^{14}\ s^{-1}$, along with the wavetrain constructed by summing the packets, each of which has a different random phase δ.

frequencies ν_i are indicated on the plot as is the boundary between the IR and visible regions, at $\nu = 4.3 \times 10^{14}\ s^{-1}$, which corresponds to a wavelength of 7000 Å. We compute a wavetrain for each field component separately by summing sequential wavepackets with random phases and assume that the amplitude, E_{ν_i}, of a wavepacket at frequency ν_i is given by

$$E_{\nu_i} = E_{\nu_i,o}\ \sin(\omega_i t + \delta)\, e^{-((t-t_{i,k})/(0.6\,\sigma_i))^2}, \tag{17}$$

where $E_{\nu_i,o}$, σ_i, and ω_i are the amplitude, Gaussian width, and circular frequency of the ith frequency component, respectively, and $t_{i,k}$ is the center time of the kth wavepacket at the ith frequency. From the requirement that $\tau_c \approx \tau_{w,i}$, where $\tau_{w,i}$ is the period for frequency ν_i, it follows that $\sigma_i \approx \tau_{w,i}$. Therefore $\sigma_i = a\,\tau_{w,i}$, where $a \approx 1$. Furthermore, it also follows that the packets are separated by an interval of $\approx\tau_{w,i}$. The kth packet is then centered at $t_{i,k}$, where $t_{i,k} = b\,k\,\tau_{w,i}$ and $b \approx 1$. Each packet overlaps with the leading and trailing packets so that the field transitions are smooth, as expected in nature. The requirement that $(a, b) \approx (1, 1)$ ensures that the overlapping wavepacket fraction is independent of frequency.

The electric field at each frequency ν_i is computed from the Poynting vector at that frequency, S_{ν_i}, given by

$$S_{\nu_i} = \Omega\, I_{\nu_i}\, \Delta\nu, \tag{18}$$

where I_{ν_i} is the solar blackbody intensity at frequency ν_i, given by

$$I_{\nu_i} = \frac{2h}{c^2}\,\frac{\nu_i^3}{e^{h\nu_i/kT_s} - 1}, \tag{19}$$

where h, k, and T_s are Planck's constant, Boltzmann's constant, and the solar photospheric temperature, respectively, and $\Delta\nu = 1. \times 10^{13}\ s^{-1}$. The units of I_{ν_i} are $W\,m^{-2}\,s^{-1}\,sr^{-1}$. An example of three consecutive wavepackets of frequency $5 \times 10^{14}\ s^{-1}$ forming a wavetrain of 1.2×10^{-14} s duration is shown in Figure 2. In this case, we assumed $(a, b) = (0.84, 1.4)$. Each packet has a different random phase δ. We plot each wavepacket separately along with the resulting wavetrain, which is computed by summing the wavepackets.

The total broadband field strength, E_t, is given by the sum of the 100 field components $E_{\nu,i}$:

$$E_t = \Sigma_1^{100}\, E_{\nu_i}. \tag{20}$$

The field components were simulated over a 1×10^{14} s period for the case: $(a, b) = (0.84, 1.4)$. In order to test the mutual

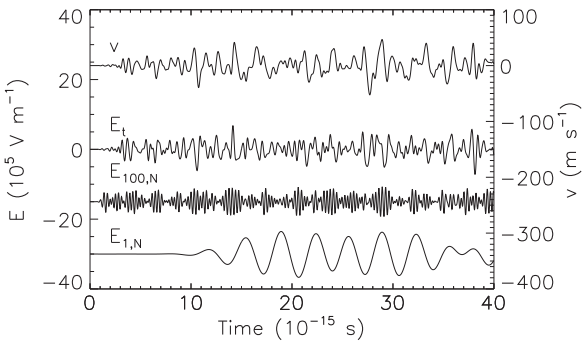

Figure 3. Plots of the normalized ν_1 and ν_{100} wave field components, $E_{1,N}$ and $E_{10,N}$, along with a plot of the total field amplitude, E_t and resulting electron velocity, v.

coherences or correlation of the field components we summed the 100 individual intensities associated with the E_{ν_i} amplitudes and integrated over the simulation period and compared that with the time integral of the intensity corresponding to the total field E_t. If the field components are mutually incoherent the two time-integrated intensities should be equal. We found that the intensity time integrals differed by less than 0.01%, indicating that the field components are uncorrelated. We corrected for limb darkening using the three parameter linear relationship in $\cos\psi$, where ψ is the angle between the Sun's radius vector and the line of sight (Cox 2000). We also computed the Fourier transform of the field and integrated the power in the 100 frequency components to verify that the 100 amplitudes matched the blackbody spectrum, which they did. The field amplitudes for frequencies $1 \times 10^{14}\ s^{-1}$, E_1 and $1 \times 10^{15}\ s^{-1}$, and E_{100} and the total field strength E_t are plotted in Figure 3. The corresponding electron velocity v was computed by integrating the momentum equation with the total field amplitude shown in Figure 3 using the third-order Adams–Bashforth numerical scheme with time steps of 5×10^{-17} s and is plotted along with the field amplitude. Note that v is strongly correlated with E_t, but does not follow the field exactly. The maximum magnitude of v is $\approx 40\ m\,s^{-1}$, but after the wavetrain, $|v| < 1\ m\,s^{-1}$, so that a change in speed over the wavetrain duration is not apparent on the plot.

4.2. Coronal Radiative Heating Simulation

To investigate coronal electron velocity diffusion in the solar radiation field, we consider an ensemble of 1000 electrons, simulate the low coherence wave field strength for each electron for several cases consistent with the requirement that $(a, b) \approx (1, 1)$, and integrate the momentum equation as in the above demonstration. We then measure the heating rate by computing the mean electron kinetic energy as the distribution evolves.

We may ignore the effect of collisions if the times for electron–electron and electron–proton collisions, τ_{ee} and τ_{ep}, respectively, are much longer than the effective coherence time. Consider the collision rates at the coronal base where the density is greatest, $2 \times 10^8\ cm^{-3}$, and the rates are largest. The electron–electron collision rate ν_{ee} is given by $\nu_{ee} = 2.9 \times 10^{-6}\, n_e\, \Lambda_c\, T_e^{-3/2}\ s^{-1}$ (Braginskii 1965) where n_e is the electron density in cm^{-3}, Λ_c is the Coulomb logarithm, and T_e is the electron temperature in eV. The collision time is given by $\tau_{ee} = \nu_{ee}^{-1}$. For a typical coronal temperature of 2×10^6 K, or 190 eV, $\Lambda = 15$ and $\tau_{ee} = 7. \times 10^{-3}$ s. The electron–proton collision time is given by $\tau_{ep} = 2\,\tau_{ee}$. Thus, the collision times are much larger than τ_c, and therefore, we may ignore particle collisions.

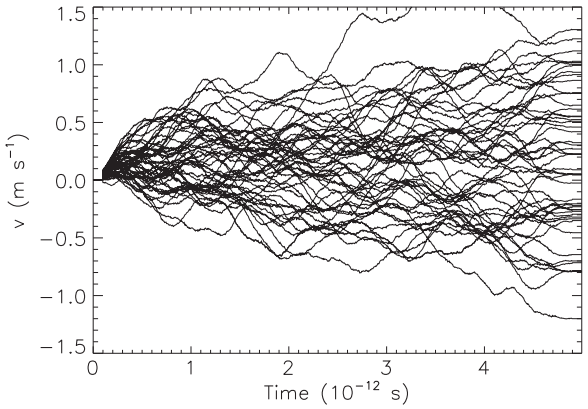

Figure 4. Plots of the averaged one-dimensional velocities $\langle|v|\rangle$ of 50 electrons driven by the simulated solar radiation field vs. time.

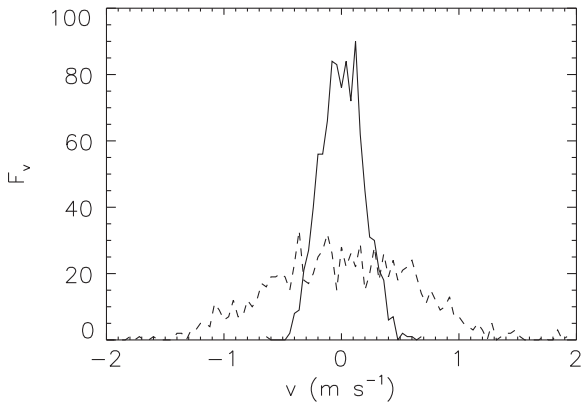

Figure 5. Plots of the one-thousand-electron one-dimensional distribution function F_v at 5×10^{-13} s (solid) and 4.5×10^{-12} s (dashed).

The heating simulations were carried out over 5×10^{-12} s, or 5 ps. These required 10^5 time steps of 5×10^{-17} s. Computation time varied from 8 hr to 15 hr and depended upon the choice of wavepacket parameters (a, b), which determined the number and widths of wavepackets in the wavetrain. The simulation began with each electron at rest. The variations in velocity caused by radiation-driven diffusion were less than $1\,\mathrm{m\,s^{-1}}$ over the simulation period, which were much smaller than the fluctuations caused by the random wave fields demonstrated in the plot of v shown in Figure 3. As such, the effects of diffusion are not apparent without significant averaging of the velocities. We smoothed the velocity curves by applying two consecutive 2×10^{-13} s wide box car filters to reduce the fluctuations, which made the smaller variations caused by diffusion apparent.

Four heating simulations spanning the (a, b) parameter ranges of (0.8, 1.2) were performed, consistent with our requirements. Plots of 50 representative averaged electron velocities $\langle|v|\rangle$ versus time for the case $(a, b) = (1.0, 0.8)$ are shown in Figure 4. Note that after averaging, the velocity fluctuation levels are $\approx 0.25\,\mathrm{m\,s^{-1}}$, as compared with the $\approx 40\,\mathrm{m\,s^{-1}}$ fluctuations in the unsmoothed velocity. The velocity curves in Figure 4 demonstrate diffusion or broadening of the distribution with time, which is equivalent to heating. Plots of the velocity distribution F_v for this simulation at 5.0×10^{-13} s and 4.5×10^{-12} s computed by averaging each electron velocity over 10^4 time steps, or 5×10^{-13} s, are shown in Figure 5. These two distributions also show the radiative broadening or heating over time evident in Figure 4.

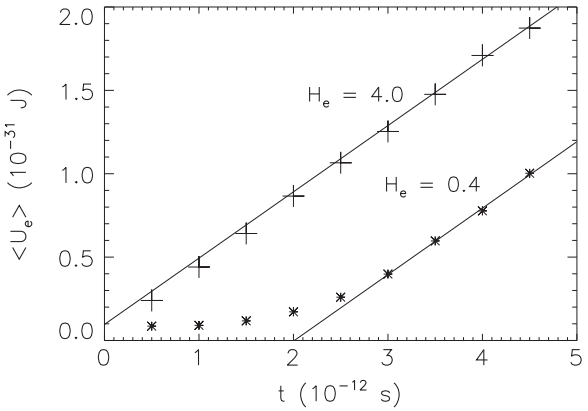

Figure 6. Plots of the average electron energies $\langle U_e \rangle$ vs. time for the case $(a, b) = (0.8, 0.8)$, (cross) and $(a, b) = (1.2, 1.2)$, $(10 \times \langle U_e \rangle)$ (star). Also plotted are lines fit to $\langle U_e \rangle$ over the heating portion of the interval for each case. The slope of each line, which equals the corresponding radiative heating rate per electron, H_e (10^{-20} W), is indicated.

The radiative heating rate per electron, H_e, was computed from the average energy for the ensemble of 1000 electrons, $\langle U_e \rangle$, over sequential periods of 10^4 time steps, or 5×10^{-13} s, as the velocity distribution broadens using Equation (5). The maximum and minimum heating rates were obtained for the (a, b) parameter cases (0.8, 0.8) and (1.2, 1.2), respectively. The heating rate increases with decreasing packet width and spacing, since they determine the smoothness of transitions between wavepackets. The sharper the transition, the greater will be the velocity kick and the heating rate. The averaged energies $\langle U_e \rangle$ computed for these two cases are plotted versus time in Figure 6. Note that for the $(a, b) = (1.2, 1.2)$ case, $\langle U_e \rangle \propto t$ with a constant slope over the simulation period, as predicted by the velocity diffusion theory presented in Section 3, while the curve for the (0.8, 0.8) case has a constant slope only for $t > 3 \times 10^{-12}$ s. In the smoother waveform case, heating begins only after a lag time. A line was fit to the entire curve in the (0.8, 0.8) case and to the portion of the curve in the interval (3×10^{-12} s $< 5 \times 10^{-12}$ s) in the (1.2, 1.2) case, in order to measure the corresponding heating rates. The (0.8, 0.8) case simulation yielded the maximum heating rate of 4.0×10^{-20} W, while the (1.2, 1.2) case yielded the minimum heating rate of 4.0×10^{-21} W. Thus, a small difference in wavepacket parameters changes H_e by a factor of 10. The heating rate obtained for the (1.2, 1.2) case, 4.0×10^{-21} W, is the minimum amount of coronal electron heating delivered by solar radiation. For comparison, the simulations were also carried out using a ten-component wave field. The resulting heating rates were larger than those yielded using a one-hundred-component field, by a factor of 1.2—a relatively small difference. Thus, the heating rates do not depend strongly on the number of field components used.

5. COMPARISON OF PREDICTED AND OBSERVED CORONAL HEATING

Radiative heating theory makes several qualitative predictions regarding coronal conditions, which we may compare with observations. First, it predicts that the heating is constant in time. This is confirmed by observations showing that temperature varies slowly, except during eruptions such as flares. Second, it predicts that heating extends everywhere in the corona at some level. This is consistent with observations showing elevated temperatures everywhere in the corona in all times, except in

some structures that are magnetically connected to the Sun, such as prominences and spicules, which have different loss mechanisms. Third, the theory predicts that the volume heating rate H_n depends on the electron density, n_e, and the heating rate per electron H_e,

$$H_n = n_e\, H_e. \tag{21}$$

This is qualitatively consistent with volume radiative loss rates which extend throughout the corona but are peaked at its base where n_e is also at a maximum.

Radiative heating theory also predicts radiative heating rates which may be compared with energy losses. There are several possible loss mechanisms: ultraviolet (UV) radiation and heat conduction and convection. Of these mechanisms, only UV radiation can be determined accurately and is known to be operating at the coronal base at all times. Thus, the UV radiation energy loss rate determines the minimum heating that solar radiation must provide. It also likely comprises the major part of coronal energy losses. These loss rates are typically given in the form of a graph of the radiative loss function F_L (W cm^3). The radiative loss rate per electron, R_e, is given by

$$R_e = n_e\, F_L, \tag{22}$$

where n_e is units of cm^{-3}. The loss function F_L depends on the elemental abundances and has been calculated for a variety of minor element fractions based on measured photospheric concentrations. A set of loss rate functions computed by various authors has been compiled by Aschwanden (2004). These rates vary between 10^{-29} W cm^3 and 10^{-28} W cm^3 for electron temperatures of 1×10^6–2×10^6 K. A more recent calculation yielded $\approx 5 \times 10^{-29}$ W cm^3 for that temperature range (Colgan et al. 2008). Coronal abundances may differ between regions, and therefore radiative loss rates might also vary with location. We will assume a nominal radiative loss function value of 5×10^{-29} W cm^3.

In the quiet corona the base electron density determined from spectroscopic UV observations equals $\approx 2 \times 10^8$ cm^{-3} (Doschek et al. 1997; Laming et al. 1997). Thus, the required volume heating rate is 1×10^{-20} W. This amount of heating is a factor of 2.5 larger than the minimum heat injected into the corona by radiation as determined by our simulations, 4.0×10^{-21} W, and is factor of 4 less than the maximum rate consistent with that requirement, 4.0×10^{-20} W. Therefore, we find that visible and IR solar radiation provide at least 40% of the power lost to UV radiation in the low corona outside of dense loops and possibly outside all of it. Thus, radiation provides at least 40% and maybe all of the heat required by more than 99.99% of the low corona volume. Since the maximum heating rate yielded by the simulations is a factor of four larger than the required quiet corona rate, radiation could also compensate for additional power losses, such as thermal conduction to the transition region and chromosphere.

The time required to heat an electron to the coronal temperature of 2×10^6 K may be computed from the radiative heating rate required to balance the radiative cooling rate. The energy corresponding to the coronal temperature is 200 eV, or 3×10^{-17} J. Assuming cooling and heating rates of 1×10^{-20} W, the heating time, τ_h, equals 3000 s. Assuming that the mean kick frequency equals the mean wave frequency of 2×10^{14} s^{-1}, the number of kicks required equals 6×10^{17}. We may estimate the mean kick magnitude using Equations (1) and (10). Given a heating rate of 1×10^{-20} W, the velocity diffusion coefficient is given by $D_v = 2.5 \times 10^9$ m^2 s^{-1}. Therefore, given a mean step time of 5×10^{-15} s, the velocity kick is given by $\delta v = 9.0 \times 10^{-3}$ m s^{-1}, or 0.9 cm s^{-1}.

Solar radiation will also provides some heat to the magnetic flux loops observed in the UV in active regions. These flux loops, which comprise less than 0.01% of the coronal, have electron densities that are higher than quiet coronal values by a factor of 1–100, as measured using UV observations. The largest densities measured in the loops are $\approx 2 \times 10^{10}$ cm^{-3} (Tripathi et al. 2009; Warren & Brooks 2009; O'Dwyer et al. 2011). Therefore, volume radiative heating rates in loops are also higher by the same factor. Since the maximum rates yielded by our simulations are a factor of four larger than those required in the quiet corona, it seems possible that radiation could heat loops with densities up to 8×10^8 cm^{-3}. Radiative heating of these structures would be consistent with the computed vertical loop heating profiles which show a peak at the footpoints (Aschwanden 2001a; Aschwanden et al. 2001). Since the volume heating rate is proportional to density, a peak at the footpoint would be expected for radiative heating. In that case, the excess heat provided to the quiet corona may be conducted to the chromosphere.

The low-density open magnetic field regions known as coronal holes will also heated by solar radiation. For a given heliocentric radius above the base, the density in holes is lower than that in the surrounding corona (Wilhelm et al. 1998; Dwivedi et al. 2000). Therefore, radiative losses there are less, and radiative heating can provide more than enough heat to explain coronal hole temperatures. The logical destination of the surplus radiative power is the fast solar wind, which originates in these regions (Krieger et al. 1973). Electron thermal energy gained from radiation may be converted into gravitational and kinetic proton energy, thereby powering the fast solar wind.

We may compute the cross section for radiative heating at the coronal base, $\sigma_{\rm rh}$, from the intensity, S_0, and the heating rate, H_e, assuming that it balances the radiative losses:

$$\sigma_{\rm rh} = \frac{H_e}{S_0}. \tag{23}$$

Given the coronal base values of S_o, 6.6×10^7 W m^{-2} and H_e, 1.0×10^{-20} W, the cross section for radiative heating may be computed: $\sigma_{\rm rh} = 1.0 \times 10^{-28}$ m^2. The minimum solar radiation power flux absorbed by the corona through heating, P_h, can be estimated from the integral of the volume loss rate:

$$P_h = \int n_e^2\, F_L\, dr, \tag{24}$$

where the integral extends over the range $(R_\odot, \infty)$. We assume that the density follows an exponential dependence on r, with a scale height l_d given by $l_d = (3\,k\,(T_e + T_p)/(m_p\, g_s)$, where g_s is the gravitational acceleration at the surface, k is Boltzmann's constant, and T_e and T_p are the coronal electron and proton temperatures, respectively, estimated at 2×10^6 K. The scale height can be evaluated: $l_d \approx 1.8 \times 10^8$ m. The required power can then be estimated: $P_h = n_{e,o}^2\, F_L\, l_d$, where $n_{e,o}$ is the base density. This yields a power level of $P_h = 810$ W m^{-2}, as compared with the base radiant flux of 7×10^7 W m^{-2}. Therefore, P_h is a factor of $\approx 10^{-5}$ lower than the radiant power density. Radiative heating will convert a small fraction of the visible and IR continuum radiation into UV line emission, which might have implications for the Sun–Earth connection. The

power absorbed by the corona will vary with the solar cycle as the density varies and may contribute slightly to solar visible and IR radiation variations.

6. CONCLUSION

We find that solar electromagnetic radiation can provide sufficient heat to explain coronal temperatures under the assumption that the optical coherence time is approximately equal to the wave period. To summarize the predictions of the coronal and chromospheric stochastic radiative heating model: (1) the radiative heating rate per electron is constant in time but varies with heliocentric distance and the volume heating rate is proportional to electron density, and (2) the radiative heating rates per electron at the coronal base yielded by our Monte Carlo simulation range from 4.0×10^{-21} to 4.0×10^{-20} W. The minimum radiative power delivered equals at least 40% and possibly all of that required to balance radiative losses outside of dense magnetic flux loops, which comprise at most 0.01% of the coronal volume. Thus, the region which could be heated by radiation includes at least 99.99% of the corona. However, it cannot supply the amount of heat required by dense loops.

7. DISCUSSION

The basic explanation for coronal heating by sunlight is twofold: (1) the Sun is a very bright light source, and (2) coronal densities are low enough that radiative losses are relatively weak. In addition to these reasons, other key contributing factors are the low mass of the electron, which allows the radiation electric field to accelerate it; and the temporal and spatial randomness in the low coherence wave field, which results from the partial coherence of sunlight. If the light from the Sun were perfectly coherent in space and time, electrons would oscillate in its radiation field indefinitely at a velocity amplitude of $\approx 40\ \mathrm{m\ s^{-1}}$, and heating could not occur. But since sunlight is only partially coherent in space and time, the random phase changes in the field impart many stochastic velocity kicks to electrons transiting coherence zones which heat the plasma to a high temperature.

Radiative heating of the corona is analogous to radio frequency (RF) heating in some laboratory plasmas, with the main differences being the frequency range, electron density, and the optical coherence of the radiation, which determines the type of heating possible. In the corona, light has a very low level of coherence, while laboratory experiments use RF radiation which is often fully coherent. In some RF-heated plasmas, electrons diffuse in velocity space because of collisions, which decouple the particle oscillation from the field (e.g., Kaganovich et al. 1996). This is essentially the mechanism proposed by Tsiklauri & Pechhacker (2011) to model partial radiative heating of the solar chromosphere. Turbulence has also been considered as a mechanism to introduce randomness to the wave–particle interaction and allow heating (Geller 1996). In the corona, collisions and turbulence are not required to explain heating, owing to the intrinsic spatial and temporal randomness in the low coherence wave field.

We have found that the minimum amount of heat deposited in the Sun's corona by electromagnetic radiation from the photosphere is sufficient to balance at least 40% of the radiation losses at quiet coronal base densities. Therefore, we expect that any sufficiently hot star will be surrounded by a hot corona with temperatures $\approx 10^6$ K. The density within the star will decrease with distance from its center until a point at which the plasma is optically thin to visible radiation. The atmosphere at that height is defined as the photosphere and the temperature there is the stellar blackbody temperature. The photosphere will radiate strongly outward. Above this height, the density decreases exponentially through the chromosphere, which is heated by electromagnetic radiation, but does not reach 10^6 K temperatures because the density n_e and the radiative losses are too large. Since the volume radiative heating rate is proportional to n_e and the volume radiative loss rate is proportional to n_e^2, n_e will fall to a level at which heating can balance cooling at a high temperature. The point at which radiative heating and losses balance is the inner boundary of the hot corona.

REFERENCES

Agarwal, G. S., Gbur, G., & Wolf, E. 2004, Opt. Lett., 29, 459
Aschwanden, M. J. 2001a, ApJ, 559, L171
Aschwanden, M. J. 2001b, ApJ, 560, 1035
Aschwanden, M. J. 2004, Physics of the Solar Corona: An Introduction (Berlin: Springer)
Aschwanden, M. J., Schrijver, C. J., & Alexander, D. 2001, ApJ, 550, 1036
Braginskii, S. I. 1965, Transport Processes in a Plasma, Reviews of Plasma Physics, Vol. 1 (New York: Consultants Bureau), 205
Cayrel 1964, SAOSR, 167, 169
Cayrel 1966, J. Quantum Spectrosc. Radiat. Transfer, 6, 621
Chandrasekhar, S. 1989, Selected Papers of S. Chandrasekhar, Vol. 2: Radiative Transfer & Negative Ion of Hydrogen (Chicago: Univ. Chicago Press), 607
Colgan, J., Abdallah, J., Jr., Sherrill, M. E., et al. 2008, ApJ, 689, 585
Cox, A. N. (ed.) 2000, Allen's Astrophysical Quantities (New York: Springer)
Doschek, G. A., Warren, H. P., Laming, J. M., et al. 1997, ApJ, 482, L102
Dwivedi, B. N., Mohan, A., & Wilhelm, K. 2000, Adv. Space Res., 25, 1751
Edlen, B. 1943, Z. Astrophys., 22, 30
Geller, R. 1996, Electron Cyclotron Ion Sources and ECR Plasmas (Bristol: Institute of Physics Publishing)
Kaganovich, I. D., Kolobov, V. I., & Tsendin, L. D. 1996, Appl. Phys. Lett., 69, 3818
Krieger, A., Timothy, A., & Roelof, E. 1973, Sol. Phys., 29, 505
Laming, J. M., Feldman, U., Schuhle, U., et al. 1997, ApJ, 485, 911
Mandel, L., & Wolf, E. 1995, Optical Coherence and Quantum Optics (Cambridge: Cambridge Univ. Press), 176
Mihalas, D. 1978, Stellar Atmospheres (2nd ed.; San Francisco, CA: Freeman)
O'Dwyer, B., Del Zanna, G., Mason, H. E., et al. 2011, A&A, 525, A137
Phillips, K. J. H. 2000, Plasma Phys. Control. Fusion, 42, 113
Ridgway, S. T., & Brault, J. W. 1984, ARA&A, 22, 291
Tripathi, D., Mason, H. E., Dwivedi, B. N., del Zanna, G., & Young, P. R. 2009, ApJ, 694, 1256
Tsiklauri, D., & Pechhacker, R. 2011, Phys. Plasmas, 18, 042901
Vernazza, J. E., Avrett, E. H., & Loeser, R. 1981, ApJS, 45, 635
Warren, H. P., & Brooks, D. H. 2009, ApJ, 700, 762
Wilhelm, K., Marsch, E., Dwivedi, B. N., et al. 1998, ApJ, 500, 1023
Wolf, E. 2007, Introduction to the Theory of Coherence and Polarization of Light (Cambridge: Cambridge Univ. Press), 44